AGU PUBLICATIONS

JGR

Journal of Geophysical Research: Oceans

RESEARCH ARTICLE

10.1002/2014JC010588

Key Points:
- Accurate irradiances are computed in an ocean ecosystem model
- Biological and physical submodels are fully coupled by the light model
- Ecosystem development is compared for approximate versus accurate light calculations

Correspondence to:
C. D. Mobley,
curtis.mobley@sequoiasci.com

Citation:
Mobley, C. D., F. Chai, P. Xiu, and L. K. Sundman (2015), Impact of improved light calculations on predicted phytoplankton growth and heating in an idealized upwelling-downwelling channel geometry, *J. Geophys. Res. Oceans*, *120*, doi:10.1002/2014JC010588.

Received 14 NOV 2014
Accepted 21 JAN 2015
Accepted article online 27 JAN 2015

Impact of improved light calculations on predicted phytoplankton growth and heating in an idealized upwelling-downwelling channel geometry

Curtis D. Mobley[1], Fei Chai[2], Peng Xiu[2,3], and Lydia K. Sundman[4]

[1]Sequoia Scientific Inc., Bellevue, Washington, USA, [2]School of Marine Sciences, University of Maine, Orono, Maine, USA, [3]Now at State Key Laboratory of Tropical Oceanography, South China Sea Institute of Oceanology, Chinese Academy of Sciences, Guangzhou, China, [4]Sundman Consulting, Chandler, Arizona, USA

Abstract Ocean ecosystem models require accurate calculations of both hydrodynamics and biology; those calculations in turn require accurate calculation of in-water irradiance. Ecosystem models now achieve great accuracy in their hydrodynamical predictions, and the biological modules are becoming correspondingly sophisticated. The optical calculations are however often oversimplified, to the possible detriment of the physical and biological predictions. We used a recently developed, extremely fast radiative transfer code, EcoLight-S, to study differences in ecosystem and thermal development in an idealized upwelling-downwelling system when simple versus accurate irradiance calculations are used. The use of accurate irradiances gave up to 57% differences in chlorophyll concentrations after two weeks of simulated time, compared to predictions based on irradiances obtained using a simple exponential attenuation formula. Accurate irradiance calculations increased sea surface temperatures and decreased temperatures at depth, leading to increased stratification. Use of EcoLight-S couples the physical and biological calculations so that biology feeds back to physics, and vice versa. EcoLight-S outputs ancillary quantities such as remote sensing reflectance and in-water spectral irradiance, which can be used to validate ecosystem predictions using remotely sensed ocean color imagery or optical measurements from buoys or gliders, without the need to convert such measurements to chlorophyll values. After optimization, the ecosystem model total run times with EcoLight-S were less than 20% more than for the analytical irradiance models. We also found that the use of 24 h average irradiances gave factor-of-two differences in chlorophyll concentrations compared to the use of a diel irradiance pattern with the same 24 h average value.

1. Introduction

Radiative transfer models such as HydroLight (www.hydrolight.info) [*Mobley et al.*, 1993; *Mobley*, 1994] solve for the complete radiance distribution $L(z,\theta,\phi,\lambda)$, where z is depth (measured positive downward from zero at the mean water surface); θ is the polar angle ($\theta = 0$ refers to light traveling toward the $+z$ or nadir direction); ϕ is the azimuthal direction; and λ is the wavelength. (See *Mobley* [1994] for notation and terminology.) Solution of the full radiative transfer equation for radiances is computationally expensive. It is also unnecessary for ecosystem models because water molecules, particulate matter, and dissolved substances are assumed to be equally likely to interact with light regardless of its direction of travel. Thus, the directional information contained in the radiance is unneeded. The spectral scalar irradiance,

$$E_o(z,\lambda) = \int_0^{2\pi}\int_0^{\pi} L(z,\theta,\phi,\lambda)\sin\theta\, d\theta\, d\phi, \tag{1}$$

describes the energy content of the light field without regard to the direction of photon travel. Scalar irradiance is therefore the radiometric quantity relevant for predictions of oceanic primary productivity, photochemical reactions, and heating of water.

When computing the heating of water by absorbed light, the energy absorbed governs the rate of change of temperature. Because plane irradiance is easier to measure and model than scalar irradiance, Gershun's law,

$$a(z,\lambda)E_o(z,\lambda) = -\frac{d[E_d(z,\lambda) - E_u(z,\lambda)]}{dz}, \quad (2)$$

is usually used to rewrite the absorption of scalar irradiance in terms of the change with depth of the net irradiance $E_d - E_u$. Here $a(z,\lambda)$ is the water total absorption coefficient, and $E_d(z,\lambda)$ is the spectral downwelling plane irradiance given by

$$E_d(z,\lambda) = \int_0^{2\pi}\int_0^{\pi/2} L(z,\theta,\phi,\lambda)\cos\theta \sin\theta \, d\theta \, d\phi, \quad (3)$$

with a similar equation for the spectral upwelling plane irradiance $E_u(z,\lambda)$. Equation (2) is convenient for use in layered models because the energy absorbed within a layer is given by the change in net irradiance across the layer. Gershun's law is an approximation of the one-dimensional form of the divergence law for irradiance [*Mobley*, 1994, equation (5.36)], which reduces to equation (2) if inelastic scatter and internal sources are omitted. Previous simulations [*Mobley*, 2011a, Table 2] have shown that omitting inelastic scatter makes at most a 5% difference in *PAR*(*z*) values at depth (at 400 m in optically pure water), and usually much less (e.g., a 1% difference at 20 m in very turbid water with a Secchi depth of 3.7 m). However, including inelastic scatter triples the run time for the EcoLight code used in those studies. Given the constraint for extremely fast run times for the light calculations in ecosystem models and the need to compute $E_d(z)$ or *PAR*(*z*) with errors of order 10%, the omission of inelastic scatter is justified. Because $E_d \gg E_u$ in deep water, the upwelling plane irradiance is often ignored in equation (2), and radiant water heating is then based on models or measurements of broadband downwelling plane irradiance,

$$E_d(z) = \int_{\lambda_1}^{\lambda_2} E_d(z,\lambda) d\lambda. \quad (4)$$

Heating by short-wave radiation typically uses $\lambda_1 = 400$nm and $\lambda_2 = 1000$nm in this equation.

Photosynthesis, on the other hand, depends on the number of photons absorbed and not their individual energies. The number of photons corresponding to irradiance in energy units at a given wavelength is obtained by multiplying $E_o(z,\lambda)$ by λ/hc, where h is Planck's constant and c is the speed of light. This converts the spectral irradiance from energy units, $\mathrm{W m^{-2} n\, m^{-1}}$, to quantum units, photons $\mathrm{s^{-1} m^{-2} n\, m^{-1}}$. The photosynthetically available radiation (PAR),

$$PAR(z) = \int_{400}^{700} E_o(z,\lambda)\frac{\lambda}{hc} d\lambda, \quad (5)$$

is a frequently used measure of the total number of photons available for photosynthesis. PAR has units of photons $\mathrm{s^{-1} m^{-2}}$.

The ecosystem model employed in the present study uses Gershun's law to reformulate the optical calculations in terms of plane irradiance E_d and its broadband equivalent to PAR, computed by using $\lambda_1 = 400$ nm and $\lambda_2 = 700$ nm in equation (4). The primary production calculations are then "tuned" to account for the numerical differences in broadband irradiance in energy units and PAR in quantum units. However, this conversion is a source of error in primary production calculations because the conversion from broadband E_d to PAR depends on the spectrum of the light. Conversion factors vary from about 5.4 μmol photons $\mathrm{s^{-1} W^{-1}}$ for a blue spectrum characteristic of low-chlorophyll water to about 8 μmol photons $\mathrm{s^{-1} W^{-1}}$ for high-chlorophyll green water (values can be still higher in Case 2 waters that shift the spectrum toward redder wavelengths). Thus, the conversion from broadband E_d to PAR depends on water properties, depth, and even sky conditions. Unfortunately, many authors refer to broadband irradiance E_d as PAR, even though E_d has energy units of $\mathrm{W m^{-2}}$. We refer to E_d as broadband irradiance so as to avoid confusion with PAR, which by definition always has quantum units.

The dependence of irradiance on time (diurnal to seasonal changes), depth, and water absorption and scattering properties is usually obtained by simple analytical models. Climatological or satellite-derived data are sometimes used to provide the time dependence of the downwelling irradiance incident onto the sea surface [*Xiu and Chai*, 2014]. Early studies sometimes neglected the diurnal variation of light completely, using climatological daily-averaged values [*Oguz et al.*, 1996]. Others modeled the diurnal variablity as a sinusoidal [*Bissett et al.*, 1994; *McCreary et al.*, 2001] or sawtooth [*Evans and Parslow*, 1985] function, or used

astronomical formulas to estimate the solar radiation as a function of time [*Fasham*, 1995; *Hurtt and Armstrong*, 1996]. Errors associated with approximating or neglecting diurnal variability in irradiance will be greatest when photo-limited and photo-adaptive effects are significant.

Given a value of $E_d(0)$ at the sea surface, ecosystem models usually employ simple analytical formulas to predict broadband $E_d(z)$ within the water column from a given chlorophyll profile and the value of $E_d(0)$ [*Fasham et al*., 1990; *Hurtt and Armstrong*, 1996; *Oschlies and Garçon*, 1998; *Chai et al*., 2002; *Fujii et al*., 2007]. Such analytical models are computationally fast, but they produce estimates of irradiance that differ by factors of 3 (near the sea surface) to 10 (at the bottom of the euphotic zone, defined as the depth where PAR is 1% of the surface value) [*Zielinski et al*., 1998]. These models have factor-of-two differences in the corresponding depths of the euphotic zone. Quantitative predictions of primary production and upper-ocean thermal structure require light calculations of greater accuracy.

The depth dependence of the broadband irradiance is often expressed as a simple exponential decay function, $E(z)=E(0)\exp(-Kz)$, where K is the diffuse attenuation coefficient for broadband irradiance. The needed value of K has been obtained in various ways. *Kyewalyanga et al*. [1992] partitioned K into two terms that depend on the average cosine of the downwelling radiance and on the solar elevation, which accounts for the different path lengths associated with direct solar and diffuse light. Others [*Fasham*, 1995; *Oguz et al*., 1996; *Moore et al*., 2002] modeled the contributions to the total attenuation by pure water, chlorophyll, CDOM, etc., but still neglected the spectral dependence of K. Most models assume that the attenuation rates of each component are constant with depth [*Evans and Parslow*, 1985; *Hurtt and Armstrong*, 1996; *Kyewalyanga et al*., 1992]. However, surface boundary effects prevent K from being constant with depth, even in homogeneous water [*Morel*, 1988]. *Moore et al*. [2002] used depth-averaged irradiances over the mixed layer. *Ohlmann and Siegel* [2000] used HydroLight simulations to develop a depth-dependent $K(z)$ as the sum of terms for water, chlorophyll, sun zenith angle, and cloud fraction. Water preferentially absorbs some wavelengths while transmitting others. Thus, the use of a wavelength-independent K can cause significant errors near the surface, where K changes most rapidly because of surface boundary effects. Errors generated near the surface then propagate with depth. *Morel and Antoine* [1994] developed a spectrally dependent model for $K(z,\lambda)$ as a sum of terms for water and phytoplankton.

Simpson and Dickey [1981] evaluated models of the downwelling irradiance over the entire spectrum according to the mathematical form of the models (simple exponential, bimodal, arctangent, and multiband). *Zielinski et al*. [1998] used the same model categories to evaluate the influence of irradiance models on ecosystem predictions made by a one-dimensional (depth dependent) bio-physical model forced by observed external irradiances. However, their comparison and conclusions were somewhat limited by the lack of measurements of the actual in-water irradiance.

It is often assumed that open ocean waters are Case 1, meaning that the absorbing and scattering properties of the water, hence K, can be parameterized by the chlorophyll concentration, which is generally a predicted state variable of biological models. However, even open ocean waters are often Case 2 [*Lee and Hu*, 2006], as are coastal waters because of resuspended sediments or terrigenous particles and dissolved substances that do not covary with chlorophyll. Also, in coastal waters, the bottom may be shallow and reflective enough for bottom reflectance to contribute significantly to the in-water scalar irradiance and upwelling plane irradiance. In order to simulate Case 2 and optically shallow waters, ecosystem models must incorporate irradiance models that are applicable to any water optical properties, depth, or bottom type.

The Ecosystem Light Subroutine (EcoLight-S) radiative transfer code [*Mobley*, 2011a] was developed to address the need for accurate but computationally fast irradiance calculations in any water body (Case 1 or 2, deep or shallow). EcoLight-S is similar in its computational algorithms to the HydroLight radiative transfer model (www.hydrolight.info) [*Mobley et al*., 1993; *Mobley*, 1994]. However, EcoLight-S is a modular package designed to be imbedded into an ecosystem model to bring the optical calculations up to the level of accuracy and sophistication found in the latest hydrodynamical and biological models. *Fujii et al*. [2007] used an early version of EcoLight-S in simulations of an equatorial Pacific upwelling region. They found that improved light calculations help constrain ecosystem behavior and give predictions consistent with

observations. They however did not optimize EcoLight-S to minimize run times while maintaining accuracy of the computed irradiances.

In the present work, we incorporate EcoLight-S into a hydrodynamical-biological ecosystem model. We compare the model performance when the default analytical irradiance models previously used for the thermal and biological calculations are replaced by EcoLight-S. We first briefly describe the hydrodynamical and biogeochemical models, and then EcoLight-S and the coupled model. We then compare the predictions made for idealized ecosystem simulations when using the original analytic light models with those made using EcoLight-S.

2. The Ecosystem Model

Our ecosystem model has separate submodels for the hydrodynamical, biogeochemical, and optical components, which we describe in turn.

2.1. The ROMS Hydrodynamical Model

We use the Regional Ocean Modeling System (ROMS) as our hydrodynamical module. ROMS [*Shchepetkin and McWilliams*, 1998, 2003, 2005] is widely used for simulations of both coastal and open ocean circulations and for coupled physical-biological applications [e.g., *Dinniman et al*., 2003; *Lutjeharms et al*., 2003; *Marchesiello et al*., 2003; *Peliz et al*., 2003; *Fennel et al*., 2006, 2008; *Fennel and Wilkin*, 2009; *Cahill et al*., 2008; *Xiu and Chai*, 2012, 2014]. ROMS gives accurate predictions of tracer fields, which is valuable for biogeochemical modeling because it facilitates accurate interaction among tracers and accounting for total nutrient and carbon budgets.

The present study used an idealized three-dimensional (3-D) channel geometry with wind forcing that generates upwelling at one side of the channel and downwelling at the other. Figure 1 shows the cross-channel geometry. The channel is 80 km wide, and the depth varies from 25 m at the channel edges to 150 m in mid-channel. The ends of the channel had periodic lateral boundary conditions so that the channel is essentially infinitely long. The circulation is thus 3-D, but computed quantities vary spatially only with depth and cross-channel location. The computational grid, shown by the black lines, has 16 terrain-following (sigma coordinate) depth layers whose thickness varies from 1.6 m at the surface near the channel edges to 22.6 m at the bottom in mid-channel. There were 80 cross-channel and 40 along-channel grid points, each of 1 km spacing. Wind forcing was applied so as to generate upwelling at the right and downwelling at the left of the channel as shown in the figure. The ROMS time step for computational stability was 5 min.

This idealized channel geometry was chosen for the present study because it allowed for short run times during code development while still retaining the full 3-D computational capabilities of physical-biological simulations. This geometry, however, is not suitable for long-term simulations.

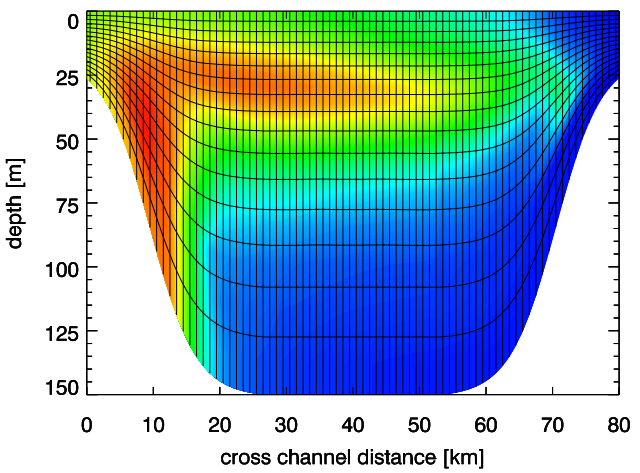

Figure 1. The cross-channel geometry. Black lines are the computational grid. Upwelling is to the right, downwelling to the left. The colors illustrate the cholorphyll concentration at a particular time.

ROMS computes water heating by a combination of short and long-wave radiation terms. The short-wave heating rate in a layer of water between depths z_1 and z_2 is computed by combining Gershun's law (2) with the first law of thermodynamics to obtain

$$\frac{\partial T}{\partial t} = -\frac{1}{\rho c_v}\frac{\partial (E_d - E_u)}{\partial z} \approx -\frac{1}{\rho c_v}\frac{E_d(z_2) - E_d(z_1)}{z_2 - z_1}, \quad (6)$$

where T is temperature (°C), t is time (s), $\rho = 1025\ \mathrm{kgm}^{-3}$ is the density of sea water, $c_v = 3900\ \mathrm{J(kg^{\circ}C)}^{-1}$ is the specific heat of sea water, and E_d is the

short-wave irradiance in Wm^{-2} defined as in equation (4). The standard version of ROMS obtains E_d from the empirical model of *Paulson and Simpson* [1977]:

$$E_d(z, 400-1000) = E_d(0, 400-1000)\left[Re^{-z/\zeta_1} + (1-R)e^{-z/\zeta_2}\right]. \quad (7)$$

R, ζ_1, and ζ_2 are parameters obtained from best fits of measured profiles of $E_d(z, 400-1000)$ in five different water types, which themselves were classified by the Jerlov water type [*Jerlov*, 1976]. The argument 400–1000 refers to the wavelength range from 400 to 1000 nm. The Jerlov water type is correlated with the chlorophyll concentration in Case 1 waters [*Morel*, 1988], and these parameters are available only for Jerlov water types I (very clear water with $Chl \approx 0.01\ mg\ m^{-3}$), IA, IB, II, and III (Case 1 water with $Chl \approx 1.5$ to $2\ mg\ m^{-3}$). We refer to equation (7) when used in equation (6) as the analytic light model for heating.

Use of the Paulson and Simpson model for higher chlorophyll values, Case 2 waters, or optically shallow waters is inappropriate. It is also noted that the use of equation (6) implies that all energy absorbed in a layer goes into heating. This is not strictly true because some of the energy is absorbed by phytoplankton or CDOM and goes into nonheat-producing chemical reactions. However, over the 400–1000 nm band for which equation (6) is used in ROMS, more than 97% of the energy absorbed by the surface layer results in heating by the water in Case 1 water with $Chl < 10\ mg\ m^{-3}$. At depths greater than roughly 1 m, the irradiance is negligible for wavelengths greater than 700 nm because of the high absorption by water. The energy absorbed in the 400–700 nm range by water itself can then be less than that absorbed by phytoplankton and CDOM, but the heating rates are much smaller than for the surface layer. Thus, the use of equation (6) is a reasonable approximation, so long as accurate irradiances are used.

The long-wave heating by infrared radiation is confined to the upper-most layer of the computational grid because of the high absorption by water itself. This term is adequately modeled in ROMS. In the studies below, we will compare short-wave heating based on equation (7) with heating when $E_d(z, 400-1000)$ is computed by EcoLight-S solving the radiative transfer equation from 400 to 1000 nm.

2.2. The CoSiNE Biogeochemical Model

Our biogeochemical model is the latest version of the Carbon, Silicate, Nitrogen Ecosystem (CoSiNE) model [*Chai et al*., 2002; *Fujii and Chai*, 2007; *Xiu and Chai*, 2012, 2014]. The current version of this model, CoSiNE-31, incorporates three phytoplankton functional groups (picoplankton, diatoms, and coccolithophorids) described by three different biomass forms (nitrogen, carbon, and chlorophyll), two size classes of zooplankton, detritus, bacteria, two classes of dissolved organic matter, particulate organic and inorganic carbon, biogenic silica SiO_2 and silicate $Si(OH)_4$, phosphate PO_4, two forms of dissolved inorganic nitrogen (nitrate NO_3 and ammonium NH_4), and other components (O_2, total alkalinity, etc.), for a total of 31 state variables. The full details of CoSiNE-31 are given in *Xiu and Chai* [2014].

CoSiNE-31 computes spectral absorption and backscatter coefficients from 400 to 700 nm at 10 nm resolution. Chlorophyll-specific absorption coefficients for picoplankton and diatoms are computed as functions of the current chlorophyll-to-carbon ratio by interpolation between spectral shapes for high and low light levels, which allows for variable photo-adaptive states of these phytoplankton. Absorption by detritus and colored dissolved organic matter (CDOM) are modeled by exponential formulas in wavelength referenced to 440 nm for detritus and 410 nm for CDOM. The low and high-light limiting spectra for picoplankton and diatoms, as well as the spectra for coccolithophorids and CDOM, are shown in *Xiu and Chai* [2014, Figure 2]. Particulate backscatter is modeled by wavelength-dependent terms for small and large organic particles, and particulate inorganic carbon, plus a fixed background.

Although the absorption and backscatter coefficients are spectrally dependent, the CoSiNE primary production and photo-oxidation calculations are driven by broadband E_d in energy units ($W\ m^{-2}$) computed over the 400–700 nm range. For the simulations considered here, the default CoSiNE E_d model uses the broadband irradiance model of *Lee et al*. [2005],

$$E_d(z) = E_d(0)\exp\left[-K(z)z\right], \quad (8)$$

where $K(z)$ is the broadband diffuse attenuation rate for visible wavelengths. $K(z)$ depends on the absorption and backscatter coefficients at 490 nm and on the solar zenith angle; the full equations are given in *Lee et al*. [2005]. We refer to equation (8) as the analytic irradiance model for biology. When using this formula,

the above-surface $E_d(400-1000)$ values used for water heating in ROMS were reduced by a factor of 0.65 to obtain $E_d(400-700)$. Those values were reduced by another factor of 0.9 to obtain in-water $E_d(0)$ for use in equation (8). In the simulations below, results obtained with this E_d model will be compared with those for E_d numerically computed by EcoLight-S using the spectrally dependent IOPs.

2.3. The EcoLight-S Radiative Transfer Model

The commercially available HydroLight software (www.hydrolight.info) [*Mobley et al*., 1993; *Mobley*, 1994] can solve the radiative transfer equation (RTE) for any given water-column inherent optical properties (IOPs, namely the absorption and scattering properties), bottom depth and reflectance, incident sky radiance, and sea-surface wave state. This model provides accurate predictions of the spectral irradiance as a function of depth and wavelength, as needed for predictions of primary production, photo-oxidation, and water heating. However, HydroLight solves for the full radiance distribution and its computational times are consequently far too great to allow its incorporation into ecosystem models that require irradiance predictions at many spatial locations and times of day over long simulation times.

Mobley [2011a, 2011b] developed the Ecosystem Light Subroutine (EcoLight-S) to address the need for extremely fast solutions of the RTE within ecosystem models. Because only irradiances are needed in ecosystem models, EcoLight-S solves an azimuthally averaged version of the RTE to obtain E_d, E_u, E_o, nadir and zenith radiances, reflectances, and diffuse attenuation functions. Run time imposes severe computational constraints on light calculations in ecosystem models. EcoLight-S therefore takes the approach of running as fast as possible, subject to the requirement that it computes broadband E_d and PAR throughout the euphotic zone with an error of no more than 10%. The depth of the euphotic zone can be set by the user to be either a percentage of the surface irradiance or the depth at which the irradiance has decreased to a chosen value.

EcoLight-S requires the same IOP and boundary condition inputs as the HydroLight code, which computes the radiance distribution to the same user-defined depth at each wavelength. To speed up its calculations, EcoLight-S employs various approximations. It is necessary to solve the RTE near the sea surface to account for the effects of the surface boundary conditions (solar zenith angle in particular) on the angular distribution of the radiance. However, below a few optical depths, the diffuse attenuation $K_d(z,\lambda)$ is well parameterized by the absorption coefficient and mean cosine; in most waters, the backscatter terms of the exact $K_d(z,\lambda)$ formulation seen in *Mobley* [1994, equation (5.65)] are small compared to $a/\bar{\mu}_d$. Thus, EcoLight-S solves the RTE at a particular wavelength only to a depth where the irradiance has decreased to either a prechosen irradiance value or to a prechosen fraction of the surface irradiance at that wavelength. Below the last depth where the RTE is solved, z_k, the irradiance is obtained by extrapolation based on the water IOPs:

$$E_d(z,\lambda)=E_d(z_k,\lambda)\exp\left[-\int_{z_k}^{z}\frac{a(z',\lambda)}{\bar{\mu}_d(z_k,\lambda)}dz'\right]. \tag{9}$$

The absorption coefficient $a(z,\lambda)$ is known throughout the water column. The mean cosine of the radiance distribution at depth z_k, $\bar{\mu}_d(z_k,\lambda)$, is used at all greater depths. The approximations inherent in equation (9), namely dropping backscatter terms that are small compared to the absorption and using a constant $\bar{\mu}_d$ below the last solution depth, are justified by the speed and accuracy requirements of EcoLight-S; further discussion of this extrapolation scheme is given in *Mobley* [2011a]. Note that the RTE is solved to different depths at different wavelengths and that the solution depth at each wavelength changes with the evolving biogeochemical state of the ecosystem. Extrapolation to greater depths is computationally inexpensive and allows for prediction of irradiances to the bottom of the euphotic zone, as needed for ecosystem calculations. EcoLight-S thus avoids solving the RTE to large optical depths, which is computationally very expensive. Optical depths can be large at wavelengths greater than 600 nm, where water absorption becomes large and even shallow physical depths can be tens or hundreds of optical depths. The ROMS-CoSiNE code simulates the water column as a stack of homogeneous layers of variable thickness. Therefore, the IOPs within a given water layer are independent of depth (hence the integration in equation (9) reduces to a summation). The EcoLight-S code takes advantage of the depth independence of the IOPs within a layer to further reduce the computations needed to solve the RTE for the depth dependence of the irradiances. In addition, EcoLight-S has options to solve the RTE only at certain wavelengths and to omit calculations of quantities not needed by the ecosystem model. Likewise, inelastic scattering is omitted because it has little effect on broadband values but is computationally expensive. The end result is that PAR and E_d can be

calculated to the bottom of the euphotic zone with errors of no more than 10%, and usually less than 5%, in about 0.1 s on a personal computer. This compares to hundreds of seconds for a corresponding HydroLight run. EcoLight-S is described in full in *Mobley* [2011a, 2011b].

EcoLight-S models the wind-blown sea surface using Cox-Munk wind speed-wave slope statistics [*Cox and Munk*, 1954] as described in *Mobley* [1994, section 4.3]. It therefore accounts for the varying transmission of sky radiance into the water column as a function of wind speed, sky conditions, and solar zenith angle during the course of a day. *Mobley and Boss* [2012] have shown that the resulting net air-to-water transmission of daily averaged, broadband, clear-sky irradiance varies from less than 80% to more than 95%, depending on the latitude, day of the year, and wind speed. Accurate transmission of radiance and irradiance into the water column is necessary to initialize the in-water irradiance calculations, regardless of what irradiance model in used to propagate the surface irradiance to depth.

Quantities such as the upwelling radiance $L_u(z,\lambda)$ and the remote-sensing reflectance $R_{rs}(\lambda)$ are not needed by ecosystem models, but these ancillary quantities can be useful for ecosystem model validation. For example, the remote-sensing reflectance depends on the current state of the ecosystem (i.e., on the water IOPs), so knowing $R_{rs}(\lambda)$ allows ecosystem validation using satellite ocean color measurements without the intervening step of converting radiometric measurements into chlorophyll concentrations via imperfect R_{rs}-to-chlorophyll algorithms. In-water profiles of $E_d(z,\lambda), E_u(z,\lambda)$, and $L_u(z,\lambda)$ allow for ecosystem model validation using optical measurements obtained from moorings or gliders. Quantities such as $L_u(z,\lambda)$ and $R_{rs}(\lambda)$ are not available from the simple analytic light models used in most ecosystem models, but they are standard outputs of EcoLight-S.

2.4. The ROMS-CoSiNE-EcoLight Coupled Model

The ROMS and CoSiNE models were previously coupled [*Xiu and Chai*, 2012, 2014], and that code served as the starting point for the incorporation of EcoLight-S. Options were added to the ROMS and CoSiNE codes so that either their default analytic irradiance models, equations (7) and (8), respectively, can be used, or those equations can be replaced by calls to EcoLight-S. Pure water IOPs were used to extend the IOPs computed by CoSiNE to 1000 nm for use by EcoLight-S; the Radtran sky irradiance code [*Gregg and Carder*, 1990] was likewise extended to 1000 nm.

When EcoLight-S is called at a particular computational grid point and time step, CoSiNE passes to it the current IOPs as functions of depth and wavelength, boundary conditions (solar zenith angle, incident sky irradiance, wind speed, and bottom depth and reflectance if applicable), and grid information (the layer depths z_i where irradiances are required for use in equation (6)). The analytic biological irradiance model of equation (8) requires only absorption and backscatter at 490 nm. EcoLight-S, on the other hand, requires a full set of spectral IOPs. To obtain the scattering coefficient, the particle backscatter coefficients computed by CoSiNE for the three phytoplankton components are rescaled using assumed backscatter fractions for each component to obtain the particle scattering coefficient. After adding water contributions, the total backscatter fraction $b_b(z,\lambda)/b(z,\lambda)$ is used within EcoLight-S to compute a Fournier-Forand scattering phase function as described in *Mobley et al.* [2002]. After solving the RTE from 400 to 1000 nm at 10 nm resolution, EcoLight-S returns both the spectral quantities obtained during the solution of the RTE ($E_d(z,\lambda), L_u(z,\lambda)$, etc.), and the broadband quantities needed by ROMS and CoSiNE. $E_d(z,400-1000)$ and $E_u(z,400-1000)$ are used in equation (6) to compute water heating without the need to neglect upwelling irradiance. $E_d(z,400-700)$ is used to replace equation (8) within CoSiNE.

It must be emphasized that when using the analytic irradiance models in ROMS (equation (7)) and CoSiNE (equation (8)), the water heating and biology are computed by two different light models. This is philosophically inconsistent even if the numerical values happen to be consistent in a particular simulation. Moreover, the separate light models within ROMS and CoSiNE allow for water heating (and the resulting effects on circulation and stratification) to influence the biological calculations within CoSiNE, but changes in the biogeochemical state of the ecosystem do not feedback to ROMS. Biology and physics are thus uncoupled. When these two equations are replaced by values computed by EcoLight-S, both water heating and biology are driven by the same light model and changes in the biogeochemical state of the ecosystem feed back to the heating calculations. Physics and biology are then fully and consistently coupled. This is shown in the flowcharts of Figure 2. The top flowchart outlines the optical

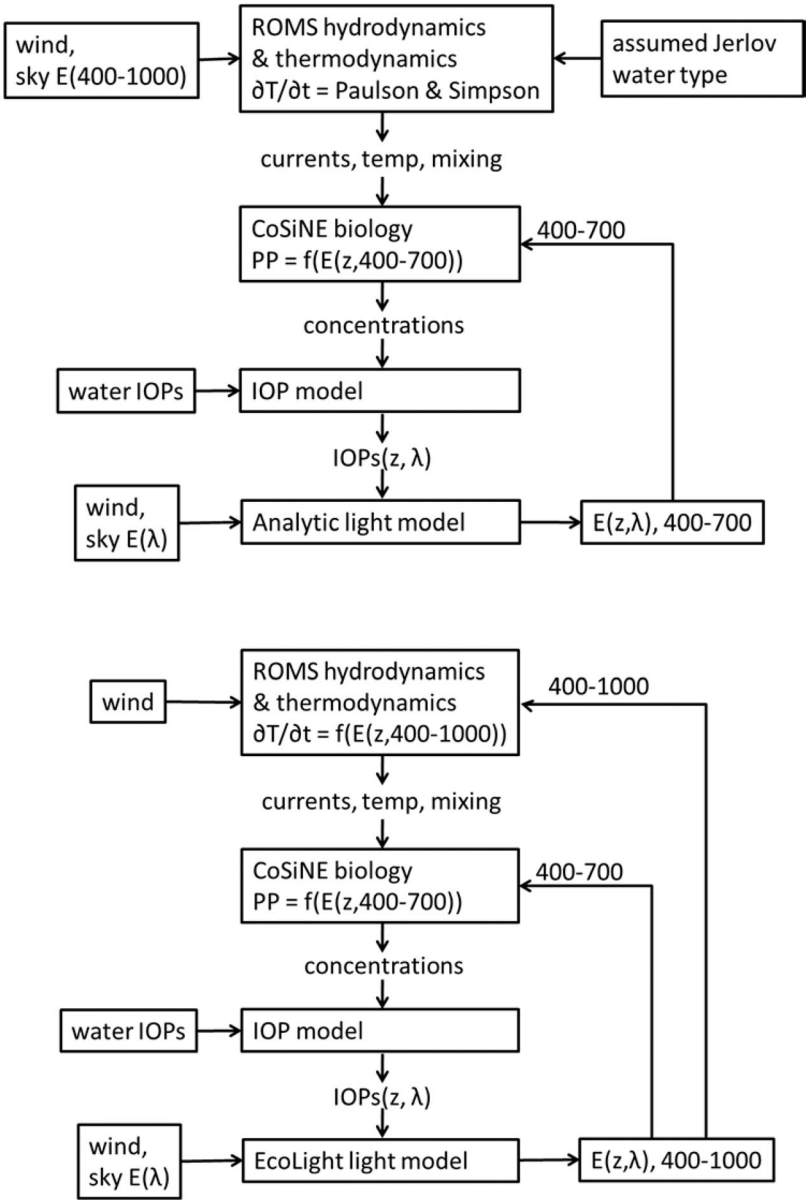

Figure 2. (top) Flowchart for light calculations in the standard ROMS-CoSiNE model. (bottom) Flowchart for light calculations in the coupled ROMS-CoSiNE-EcoLight code. $\partial T/\partial t$ represents calculation of temperature changes by absorption of short-wave radiation; PP represents primary production and other biological calculations within CoSiNE.

computations in the standard ROMS-CoSiNE code. In that code, the assumed Jerlov water type is held fixed during the entire simulation, regardless of how the water optical properties change with changing biogeochemistry. The bottom flowchart shows that EcoLight-S computes spectral E_d from 400 to 1000 nm. The full wavelength range is used to compute $E_d(z, 400-1000)$ to replace the Simpson and Paulson values within ROMS. The 400–700 nm range is used to compute $E_d(z, 400-700)$ to replace the analytic irradiance model within CoSiNE.

3. Ecosystem Simulations

We now present results for ecosystem simulations using various irradiance models and ecosystem parameter values. We adjusted phytoplankon maximum growth rates, mortality rates, and sinking speeds; zooplankton grazing dynamics; and initial nutrient concentrations so as to allow the development over 2 weeks of low (∼0.5), medium (∼2), and high (∼5 mg Chl m^{-3}) chlorophyll concentrations.

3.1. Initial Conditions and External Forcing

The initial conditions and parameter values used for these simulations are given in Table 1. Figure 3 shows the initial conditions for total chlorophyll (the sum of chlorophyll for the three phytoplankton components), nitrate, and temperature for the high-chlorophyll simulation. Chlorophyll is given a value of 0.24 mg m^{-3} throughout the water column for all simulations. Nitrate ranges from 5 mmol N m^{-3} at the surface to 6.8 mmol N m^{-3} at the mid-channel bottom for the medium and high-chlorophyll simulations, and 2.5–3.4mmol N m^{-3} for the low-chlorophyll simulation. Temperature ranged from 14°C at depth to 21.9°C at the surface.

Spectral irradiance incident onto the sea surface, $E_d(\text{air}, \lambda)$ was computed using the Radtran sky irradiance model run from 400 to 1000 nm by 10 nm resolution and for an approximately 12 h day-night cycle. The sky had a 30% cloud cover. The diel cycle of sky irradiance was for a location at 34°S.

A wind stress of 0.1 N m^{-2} was applied in the along-channel direction; this stress corresponds to a wind speed of about 8.5 m s^{-1}. This wind generates a cross-channel surface flow due to Ekman pumping. A nearly steady state flow is reached within a few days. The cross-channel surface water speed is then about 0.08 m s^{-1}, which carries water from the upwelling to the downwelling side of the channel in about 10 days.

The bottom right plot of Figure 3 shows the diel pattern of E_d computed from the Radtran $E_d(\text{air}, \lambda)$. This pattern was repeated each day, except for a small difference due to the changing day of the year over the 2 week simulation period. This diel irradiance was used to compute the 24 h averages in the first simulations below.

3.2. Effects of Diel Versus Daily-Averaged Irradiances

Many ecosystem models are driven by daily-averaged irradiances even though their hydrodynamic and biological calculations are done at much smaller time intervals. We therefore first investigated the differences in ecosystem development when using a constant 24 h average irradiance versus a diel pattern having the same 24 h average. In both cases, the hydrodynamics and biogeochemistry were updated at each of the ROMS 5 min time steps over the course of a 2 week simulation. The high-chlorophyll initial conditions and ecosystem parameter values of Table 1 were used, which allowed for the development of a plankton bloom over the 2 week simulation period.

As seen in Figure 3, the maximum daily value of the Radtran-computed $E_d(\text{air}, 400-1000)$ is 669.2 W m^{-2} versus a 24 h average of $\langle E_d(\text{air}, 400-1000)\rangle_{24} = 197.1$ W m^{-2}. The maximum of $E_d(\text{air}, 400-700)$ is 434.2 W m^{-2} versus an average of $\langle E_d(\text{air}, 400-700)\rangle_{24} = 127.4$ W m^{-2}. Comparison runs were done with these irradiances as the surface values in equations (7) and (8). The ratio of daily-averaged irradiance at PAR wavelengths (400–700 nm) to the short-wave irradiance (400–1000 nm) used for heating is 0.65 in the present case. Even after a further reduction by a factor of 0.9 to account for surface reflectance, this is more than the value of 0.46 assumed in the default ROMS-CoSiNE code to convert the ROMS short-wave irradiance into the value of $E_d(0, 400-700)$ used to initialize the analytic model of equation (8).

Table 1. Initial Conditions and Rates for the Low, Medium, and High-Chlorophyll Simulations[a]

Parameter	Units	Low Chl	Medium Chl	High Chl
Total Chl ($t = 0$)	mg Chl m^{-3}	0.24	0.24	0.24
NO_3 ($t = 0$)	m mol N m^{-3}	2.5–3.4	5.0–6.8	5.0–6.8
$Si(OH)_4$ ($t = 0$)	m mol Si m^{-3}	3.8–5.1	7.5–10.2	7.5–10.2
S1 max growth rate	day^{-1}	2.0	2.0	1.5
S1 mortality rate	day^{-1}	0.2	0.02	0.2
S1 sinking speed	md^{-1}	0.0	0.0	0.0
S2 max growth rate	day^{-1}	2.5	2.0	2.5
S2 mortality rate	day^{-1}	0.3	0.05	0.05
S2 sinking speed	md^{-1}	0.0	0.0	0.0
S3 max growth rate	day^{-1}	1.0	1.0	1.0
S3 mortality rate	day^{-1}	0.2	0.05	0.5
S3 sinking speed	md^{-1}	0.0	0.0	1.0
Z2 max grazing rate	day^{-1}	0.56	1.0	0.56
Z2 graz pref for S2	Nondimensional	0.6	0.7	0.6
Z2 graz pref for Z1	Nondimensional	0.1	0.2	0.1
Z2 graz pref for PON	Nondimensional	0.2	0.05	0.2
Z2 graz pref for S3	Nondimensional	0.1	0.05	0.1
Half-saturation for $Si(OH)_4$ by S2	m mol Si m^{-3}	4.5	8.0	4.5

[a]S1 refers to picoplankton, S2 to diatoms, and S3 to coccolithophorids; Z1 is microzooplankton; Z2 is mesozooplankton. Other model parameters not shown here were the same for each simulation and had the values shown in Table 1 of *Xiu and Chai* [2014].

The top row of Figure 4 shows the chlorophyll (left column) and temperature (right column) at noon of day 14 for the simulation with 24 h average irradiances used for water heating and biology. The second row shows the results when the diel irradiances were used. Row three gives the difference, diel − average, and row four gives the relative percent

Table 2. Comparison of Analytic (Ana) and EcoLight (Eco) Runs for Low, Medium, and High-Chlorophyll Simulations at Noon of Day 14[a]

Chl Case	Max Chl (mg Chl m^{-3})	Max Δ Chl (mg Chl m^{-3})	Max Δ Chl (%)
Low	Ana: 0.47 at (11.5, 95.2) Eco: 0.48 at (11.5, 95.2)	0.14 at (20.5, 58.7)	56.6 at (22.5, 70.3)
Med	Ana: 2.06 at (36.5, 18.9) Eco: 1.98 at (45.5, 23.9)	0.48 at (23.5, 59.8)	32.5 at (63.5, 39.3)
High	Ana: 4.64 at (9.5, 58.2) Eco: 5.02 at (8.5, 45.4)	1.07 at (22.5, 50.3)	40.0 at (70.5, 37.3)
Chl Case	Max Temp (°)	Max Δ Temp (°)	Max Δ Temp (%)
Low	Ana: 20.19 at (1.5, 29.0) Eco: 20.22 at (1.5, 7.1)	0.09 at (1.5, 5.9)	0.4 at (1.5, 5.9)
Med	Ana: 20.19 at (1.5, 29.0) Eco: 20.34 at (0.5, 7.1)	0.27 at (0.5, 5.5)	1.3 at (0.5, 5.5)
High	Ana: 20.19 at (1.5, 29.0) Eco: 20.36 at (0.5, 7.1)	0.30 at (0.5, 3.9)	1.5 at (0.5, 3.9)

[a]The top rows show the maximum values of chlorophyll and the maximum (EcoLight − Analytic) differences and the maximum percent differences, 100(EcoLight − Analytic)/EcoLight. The locations are: cross-channel distance in km, depth in m. The bottom rows show the corresponding comparisons for temperature. The maximum values for the high-chlorophyll case can be compared with the overall spatial patterns seen in Figure 5.

difference, 100(diel − average)/diel. We see that the simulation based on a diel irradiance pattern gave only one half of the maximum chlorophyll value seen in the simulation using a constant irradiance: 3.4 versus 7.8 mg Chl m^{-3} at the depth of the chlorophyll maximum in the downwelling region. The temperature on the other hand was little affected by the irradiance pattern. The differences in temperature were no more than 0.04° or 0.2%. Recall that physics and biology are not coupled when the analytic irradiance models are used; thus, the growth in phytoplankton did not affect the heating in this simulation. In CoSiNE, each phytoplankton functional group has its own photosynthesis rate versus irradiance (P versus E) curve. When the irradiance is constant, growth continues over the entire 24 h. For a diel irradiance, the phytoplankton cycle through periods of no growth at night, to maximum growth during the day, and perhaps even photoinhibition when the irradiance is highest. Phytoplankton growth rates depend on evolving nutrients and C:N and C:Chl ratios, as well as on irradiance. The large difference in chlorophyll results from the differences in growth rates for the

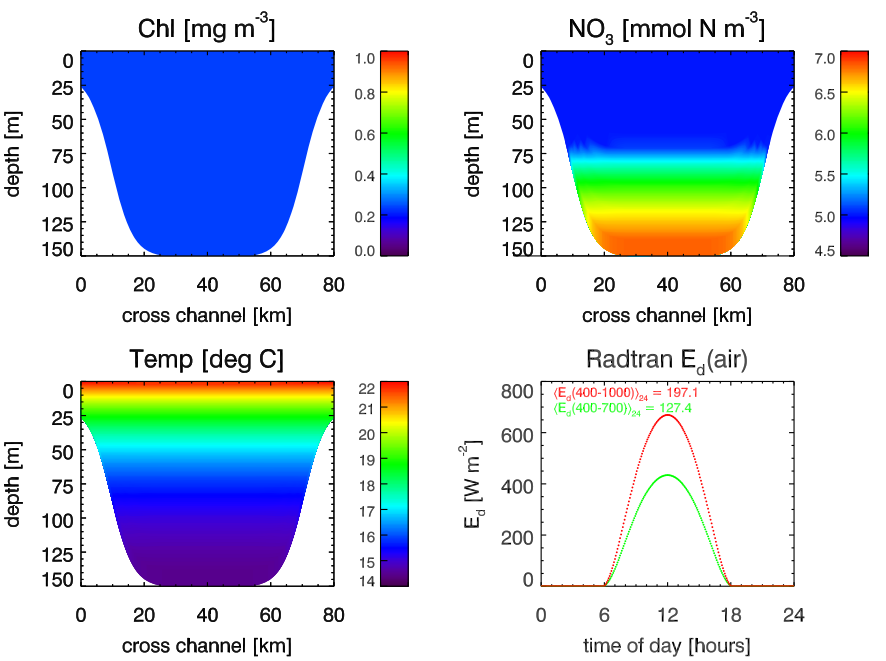

Figure 3. Initial conditions for chlorophyll, NO_3, and temperature for the high-chlorophyll case. The bottom right plot shows the diel pattern of incident E_d used to drive the simulations. The dots are at the ROMS time steps. The red curve is for 400–1000 nm, as used for ROMS water heating calculations; the green curve is 400–700 nm, as used for CoSiNE biological calculations. Initial conditions for $Si(OH)_4$ and NH_4 are shown in Figure 6. Other initial conditions are given in Table 1.

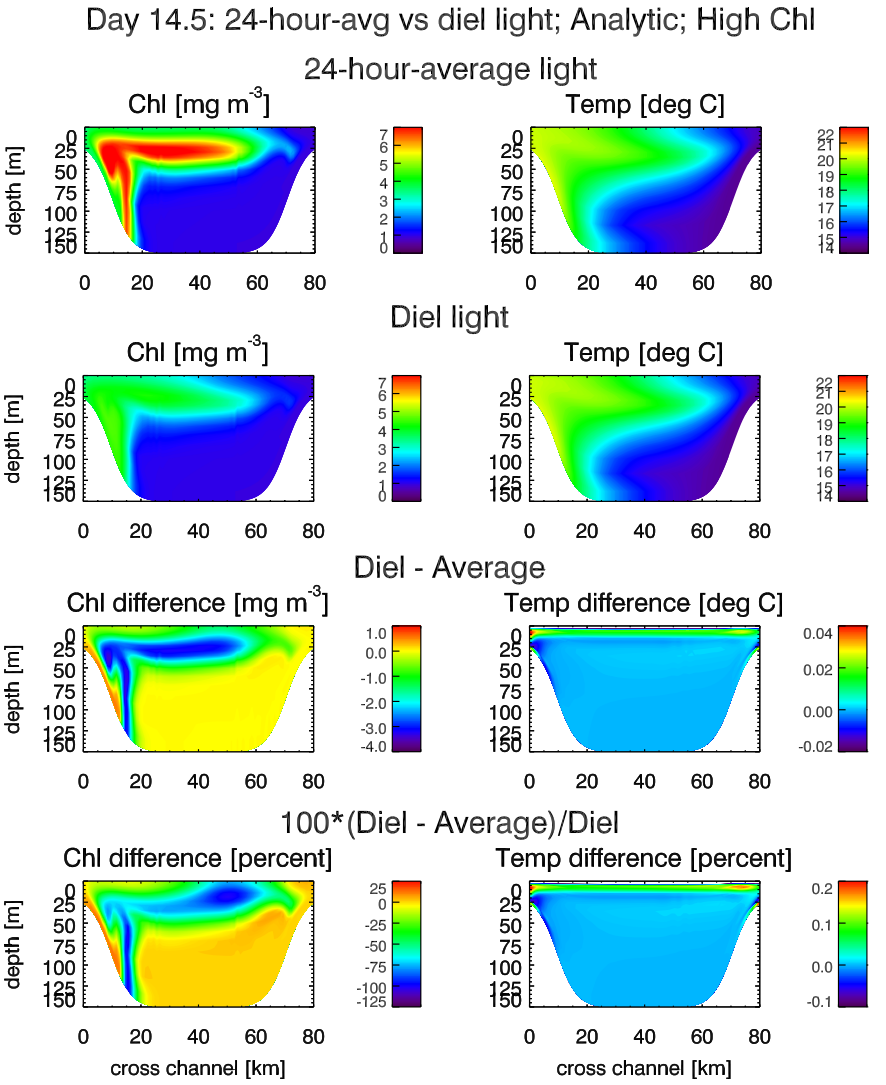

Figure 4. Ecosystem development at noon of day 14 for 24 h-average versus diel surface irradiances, for the high-chloorphyll case. The default irradiance models were used.

irradiance values applied to the P versus E curves. For temperature, it is only the total amount of energy absorbed that determines the heating during a 24 h period. There are only very small differences near the surface resulting from the pattern of diurnal heating and nocturnal cooling for the diel pattern, compared to constant rates of heating and cooling for the case of constant irradiance. We thus see that although use of daily-averaged irradiances may be acceptable for driving the hydrodynamics, this is an unacceptable oversimplification of phytoplankton dynamics and can lead to large differences (a factor of 2 in the present case) in ecosystem biology, even after just 2 weeks. *Lee et al.* [2012] reached similar conclusions about the importance of including diel irradiance dependence in biological calculations.

3.3. Effects of Analytic Versus EcoLight Irradiances

We now consider differences in ecosystem development when the analytic irradiance models of equations (7) and (8) are replaced by EcoLight-S numerically computed values. We first present the results for the high-chlorophyll initial nutrient concentrations, growth rates, grazing rates, etc. All simulations used the diel irradiance pattern seen in Figure 3.

Both ROMS and CoSiNE update their respective variables at every 5 min ROMS time step and thus need broadband irradiance profiles at this time resolution. However, it is not necessary to call EcoLight-S at every time step

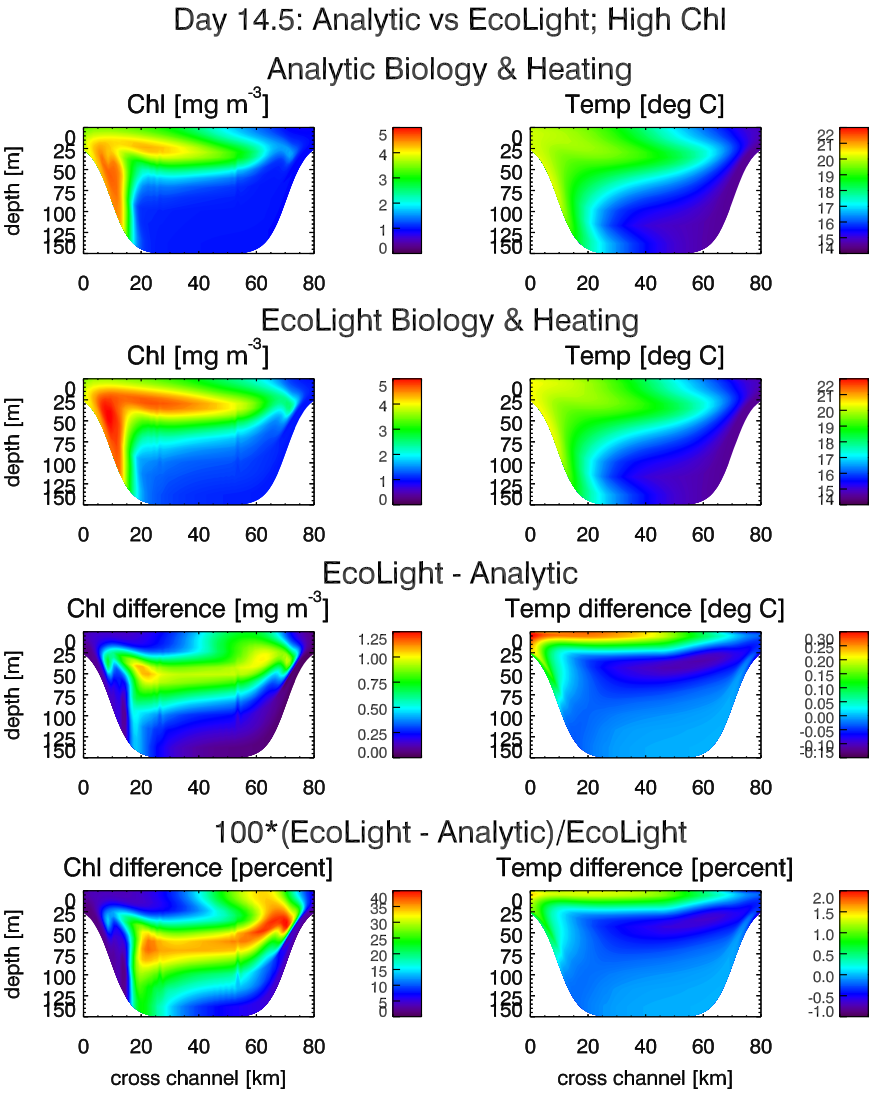

Figure 5. Ecosystem development after 2 weeks for analytic versus EcoLight-S irradiances, for the high-chlorophyll case.

to perform a complete recalculation of the in-water irradiances. Previous simulations [*Mobley et al.*, 2009] have shown that it is sufficient, even in multiyear simulations, to call EcoLight-S for a de novo irradiance calculation only every few hours of simulated time. The reason is that the in-water biological properties change very little on the scale of the ROMS computational time step, although biology can change significantly over the scale of several hours. In the following simulations, EcoLight-S was called at the first time step after sunrise, and then at 2 h intervals thereafter until sunset. For computational time steps, for which EcoLight-S was not called, the most-recently computed irradiance profiles, $E_d(z, 400-700)$ and $E_d(z, 400-1000)$, were rescaled by the corresponding change in the incident sky irradiance, which can change significantly on scales of less than 2 h. Thus, at a time t, when EcoLight-S is not called, the irradiance is given by

$$E_d(z,t) = E_d(z, t_{\text{last call}}) \frac{E_d(\text{air}, t)}{E_d(\text{air}, t_{\text{last call}})}.$$

This amounts to using the most recently computed diffuse attenuation, $K_d(z)$, which is determined by the in-water biogeochemical constituents, to compute the $E_d(z)$ profile with the current value of the input sky irradiance. Two such equations are used for the 400–700 and 400–1000 nm bands.

Likewise, previous studies [*Mobley*, 2011a] show that computing $E_d(z, \lambda)$ at 30 nm wavelength intervals down to the depth where the irradiance has decreased to 10% of its surface value at each wavelength gives

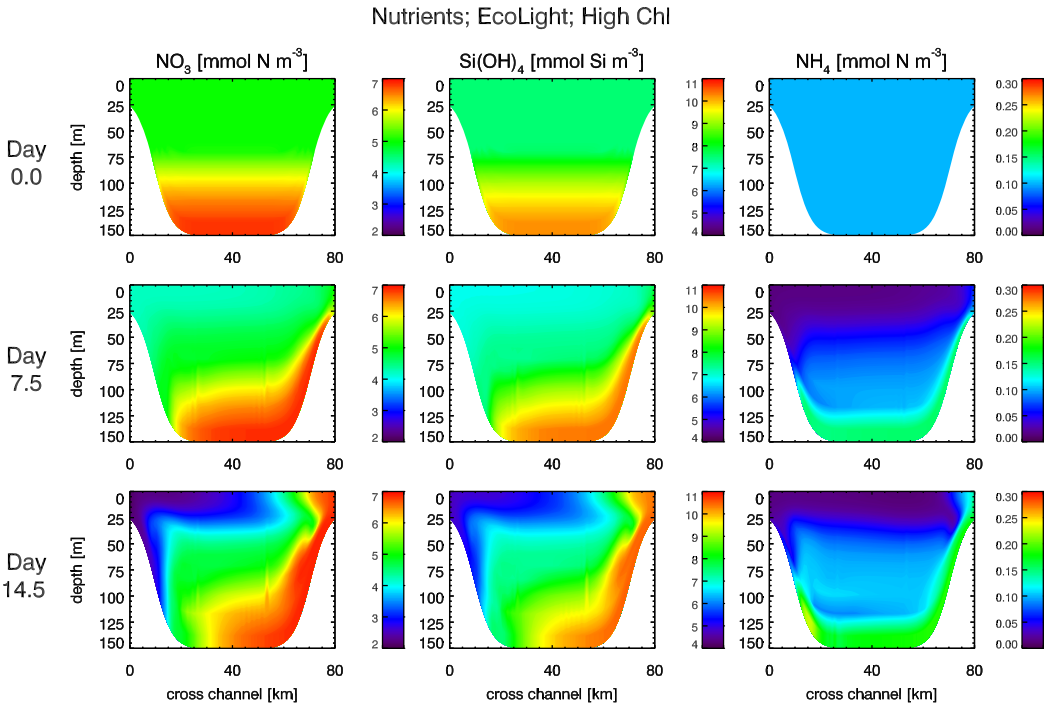

Figure 6. Nutrient initial conditions for the high-chlorophyll simulation. Values at 1 and 2 weeks are for the EcoLight-S simulation.

broadband irradiances throughout the euphotic zone that are within a few percent of the values obtained at 5 nm resolution with the RTE solved to the bottom at each wavelength. Reducing the number of wavelengths where the RTE is solved, the depth to which it is solved, and the frequency of calling EcoLight-S all

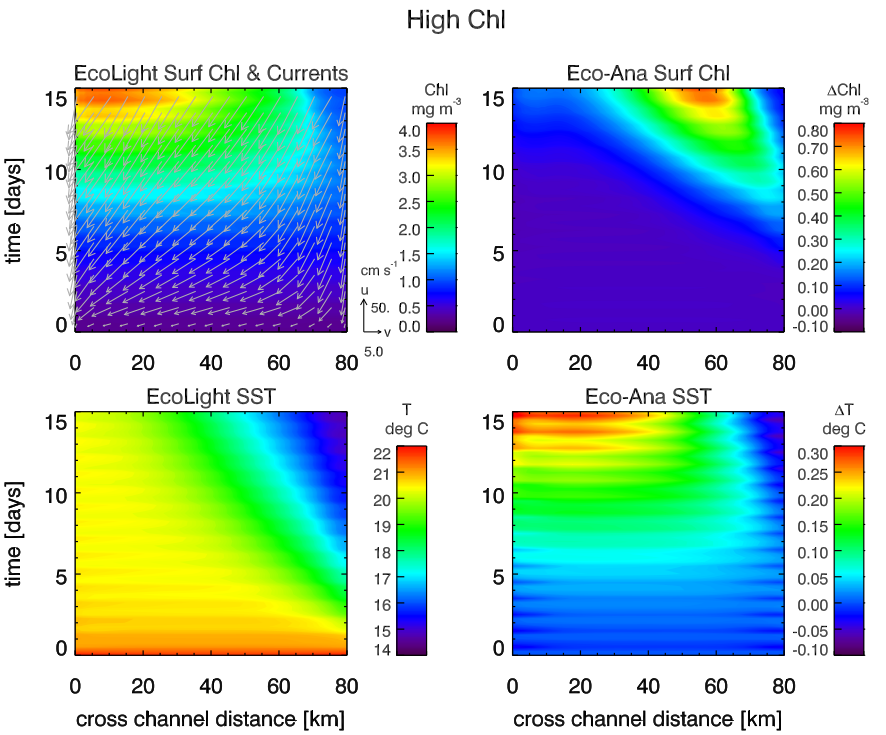

Figure 7. Time development of chlorophyll, currents, and temperature in the surface layer. Note that the surface current vectors in the top left plot have different scales for the along and cross-channel components.

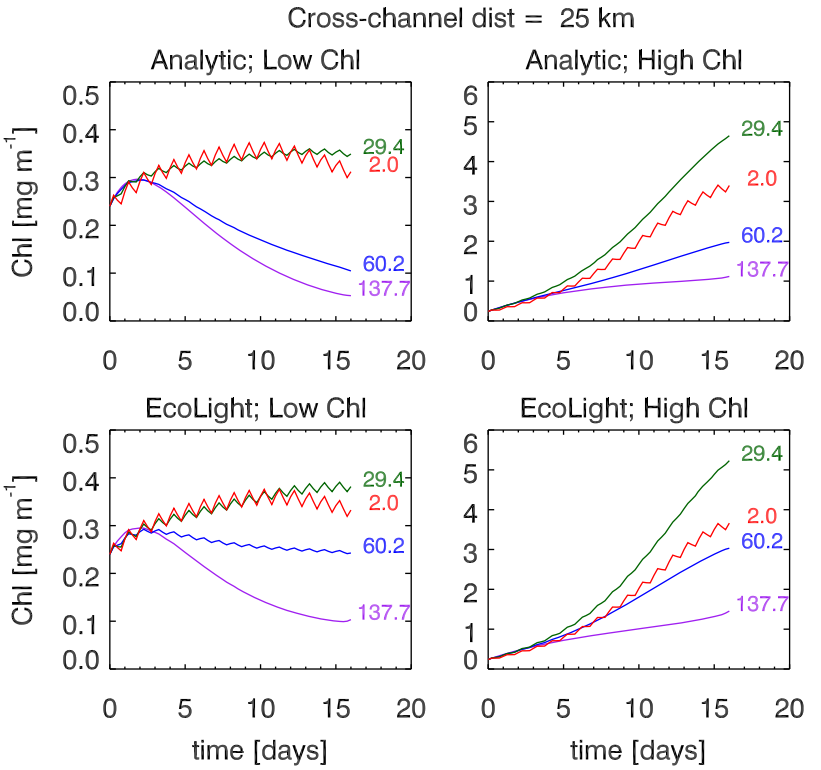

Figure 8. Time development of chlorophyll at the cross-channel location where the EcoLight-Analytic differences are greatest, for selected surface, mid-column, and bottom depths. Numbers next to the curves are the depths in meters.

reduce the total computation time. In the present simulations, EcoLight-S was called at every cross-channel grid point for one along-channel point. Those irradiances were then used at all other along-channel points because the periodic boundary conditions at the channel ends give no along-channel variability.

Figure 5 shows results at noon of day 14 for the high-chlorophyll simulation. The top row is the same as row 2 in Figure 4, but with a different scale for the chlorophyll values. The second row shows the chlorophyll and temperature when EcoLight-S is used to compute the in-water irradiances. Recall that with EcoLight-S, physics and biology are fully coupled. Thus, the changing biological state of the ecosystem feeds back to the heating calculations. The chlorophyll values computed with EcoLight-S are as much as 1.1 mg Chl m^{-3} (in the downwelling region) or 40% (in the upwelling region) greater than the values computed with the analytic irradiance model. The sea surface temperature is as much as 0.3°C warmer at the surface (in the downwelling region) with EcoLight-S, and the water is as much as 0.1° C cooler at depth (in the upwelling region). This shows the effect of the greater chlorophyll concentration absorbing more light near the surface and thus reducing the light at depth. The total run time for the simulation with the analytic irradiance models was 143 min when run in serial mode on a single-processor Linux computer. The corresponding time with EcoLight-S was 170 min. This is an increase in total run time of only 17%, which we consider a small computational price to pay for the improved light calculations.

The results are qualitatively similar for the low and medium-chlorophyll cases. The spatial patterns are similar to those shown Figure 5 and need not be shown. For the low-chlorophyll case, the chlorophyll maxima are now slightly less than 0.5 mg m^{-3}. The EcoLight-S values are as much as 0.14 mg m^{-3}, or 57%, greater (depending on location) than the values with the analytic light models. Again, the water is warmer at the surface at downwelling side of the channel, and cooler at depth at the upwelling side, although the difference in SST is now less than 0.1°C. For the medium-chlorophyll case, the maximum chlorophyll concentrations are close to 2 mg m^{-3}, and the maximum chlorophyll differences between EcoLight and analytic models are about 0.5 mg m^{-3}, or 33%, depending on location. The maximum temperature differences are again close to 0.3°. Locations of the maxima and maximum differences are given in Table 2 for all three cases. Run times for the low and medium-chlorophyll simulations were again less than 20% more for EcoLight than for the analytic light model.

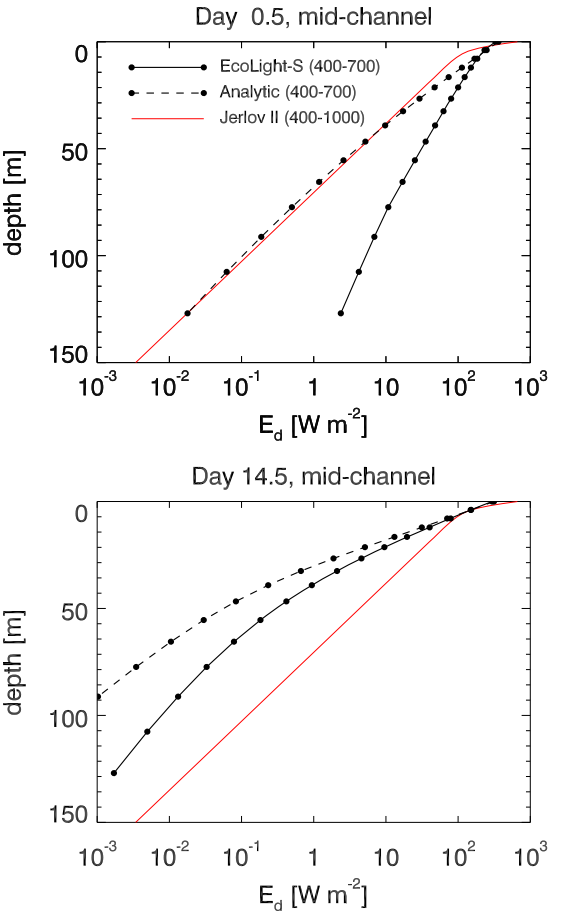

Figure 9. (top) Irradiance profiles $E_d(z, 400-700)$ for EcoLight-S and the analytic biological light model at noon of the first day and the mid-channel location (cross-channel distance 40 km). The dots show the irradiances at the layer midpoints. The curve extending to 150 m is $E_d(z, 400-1000)$ as given by equation (7) for Jerlov water type II. (bottom) The corresponding irradiance profiles at noon of day 14.

Figure 6 shows the changes in NO_3, $Si(OH)_4$, and NH_4 at weekly intervals for the high chlorophyll, EcoLight case. The upwelling of nutrients at the right side of the channel and the depletion of nutrients in the surface waters as phytoplankton are transported leftward are clear. The spatial patterns for the other simulations are similar.

The time development of the sea surface chlorophyll and temperature for the high-chlorophyll conditions as computed by EcoLight, and the EcoLight minus analytic differences, are shown in Figure 7. The maximum differences in surface chlorophyll are in the upwelling region, and the maximum temperature differences are in the downwelling region, with the EcoLight values being greater for both variables. The horizontal banding results from the day-night variations. The top left plot also shows the surface currents. For ease of visualizing the flow pattern, current vectors are plotted at only every fifth cross-channel grid point, and the along-channel and cross-channel velocity components have different scales. The maximum along-channel component is 0.67 ms^{-1}, and the maximum cross-channel component is 0.08 ms^{-1}.

Figure 8 shows time series of total chlorophyll near the cross-channel point in the downwelling region where the analytic versus EcoLight differences are the greatest, for selected surface, mid-column, and bottom depths and for the low and high-chlorophyll simulations. The near-surface chlorophyll values are similar for the analytic and EcoLight simulations because both models have the same surface irradiances. The model differences are greatest near the depth of the chlorophyll maxima because of the different attenuation rates within the water column.

The above differences in ecosystem development all result from the differences in irradiances computed by EcoLight-S and the analytic light models. The top plot of Figure 9 shows mid-channel $E_d(z, 400-700)$ profiles at noon of the first day, at which time the chlorophyll and nutrients are almost unchanged from their initial values (the first simulation day is time 0–1 days with 0 being local midnight and 0.5 being noon). Even for identical IOPs, EcoLight-S and the CoSiNE analytic light model of equation (8) give much different $E_d(z)$ profiles. In the present case with $Chl \approx 0.24\ mg\ m^{-3}$, $E_d(z)$ is greater for EcoLight-S at depths greater than 10 m, which leads to the different chlorophyll values as time goes on. The profile of $E_d(z, 400-1000)$ as given by equation (7) for Jerlov water type II (used in the analytic heating model for the present simulations) is shown for comparison. The Jerlov curve has almost the same values at depth as the analytic biological model (8) for this low chlorophyll concentration. As time goes on, the ecosystem develops according to the different light models. The bottom plot of Figure 9 shows the irradiance profiles at noon of day 14 for the high-chlorophyll case. The IOPs are now different for the two light models, but the EcoLight-S $E_d(z, 400-700)$ is still greater than the profile for the analytic model, even though the chlorophyll is somewhat greater for EcoLight-S. The default $E_d(z, 400-1000)$ remains unchanged from its initial profile, according to the assumed Jerlov water type, and is now much different from the biological light model. This illustrates the inconsistency of the analytical light models for biology and heating, and the inability of an assumed Jerlov water II to describe heating at depth all times and locations, even if it is correct on occasion (as initially, in the present case).

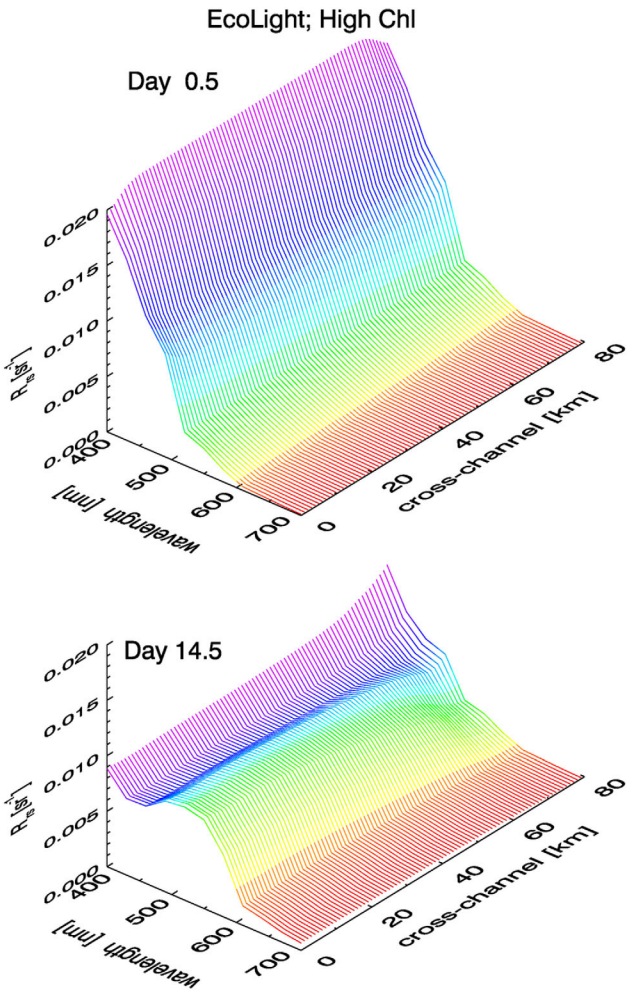

Figure 10. Cross-channel remote-sensing reflectances R_{rs} at noon of days 0 and 14 for the high-chlorophyll case.

One of the virtues of using EcoLight-S is that it provides important ancillary output that is not available from analytic light models. An example of this is the remote-sensing reflectance, R_{rs}, as shown in Figure 10. At noon of the first day, these spectra are blue at all cross-channel points, because the chlorophyll concentration is everywhere still near its initial low value of 0.24 mg m^{-3}. For the high-chlorophyll simulation shown here, the spectra at noon of day 14 show that the upwelling side of the channel still has blue spectra characteristic of low-chlorophyll water, but that the downwelling side has green spectra characteristic of high-chlorophyll water, consistent with Figure 5. These spectra are determined by the water absorption and scattering properties, which in turn depend on the biogeochemical state of the ecosystem. Such spectra therefore can be used to validate ecosystem predictions using satellite or airborne ocean-color imagery, without the need to convert the image spectra to chlorophyll concentrations (or to other measures of ecosystem state). Other EcoLight-S standard outputs such as the spectral in-water $E_d(z,\lambda), E_u(z,\lambda)$, and $L_u(z,\lambda)$ can likewise be used for model validation from optical measurements made on moorings or gliders. The availability of these optical quantities argues for the use of EcoLight-S even in situations where the analytic light models provide adequate broadband irradiances.

4. Conclusions

The results presented here are for an idealized channel geometry that was convenient for code development and proof-of-principle ecosystem simulations. Regardless of the simple geometry and limited simulation times, these results (and those of *Mobley et al*. [2009] and *Fujii et al*. [2007]) show that it is computationally feasible to incorporate accurate irradiance calculations into ocean ecosystem simulations, and that the use of accurate irradiance calculations leads to differences in ecosystem evolution.

When driven by a diel pattern in incident sky irradiance, the chlorophyll values were as much as a factor of 2 less than the values obtained by the corresponding 24 h average irradiance (Figure 4). This difference results from the diurnal cycling through the irradiance-dependent photosynthesis rates for the different phytoplankton functional types, versus continuous growth for all 24 h. Heating rates were little affected by diel versus constant irradiance forcing because it is the total amount of energy absorbed over 24 h that determines the net daily heating.

In the simulations using analytic versus EcoLight-S diel irradiances, the maximum differences in total chlorophyll were as much as 57% after only 2 weeks, depending on location. In the low-chlorophyll simulation with EcoLight-S, the chlorophyll was as much as 0.14mg m^{-3} greater in the downwelling region, compared to a

value of about 0.3mg m^{-3} for the analytic irradiance models. For the high-chlorophyll simulation, EcoLight-S values were as much as 1.1mg m^{-3} greater, compared to analytic values of about 3mg m^{-3} (Figure 5 and Table 2). Near-surface temperatures were as much as 0.3°C greater with EcoLight-S, and temperatures at depth were reduced by as much as 0.1°C. These differences result from increased absorption by phytoplankon in near-surface waters, and consequent shading of deeper waters, when the heating and biology are coupled via EcoLight-S irradiance calculations.

The use of EcoLight-S gives a number of improvements in the realism of ocean ecosystem models. First, EcoLight-S couples the biogeochemical and hydrodynamical modules of the ROMS-CoSiNE model via consistent irradiance calculations. This coupling can be done in a similar fashion for any other biogeochemical and hydrodynamical models. Because EcoLight-S solves the RTE for radiance, it automatically accounts for transmission of sky radiance (hence of irradiance) through the sea surface as a function of wind speed, solar zenith angle, and atmospheric conditions. The water-column inputs to EcoLight-S are simply the spectral absorption and scattering properties of the water body. Those IOPs can describe any water body from the clearest Case 1 water to the most turbid Case 2 water. EcoLight-S is therefore valid for use in any water body and, importantly, does not require the a priori choice of a water type as is commonly made in ROMS heating calculations. In addition, it provides ancillary outputs such as the remote-sensing reflectance (Figure 10) and in-water spectral irradiances and upwelling radiance, which can be used to validate ecosystem predictions via remotely sensed or in-water optical measurements without the need to covert the optical measurements to chlorophyll or other biogeochemical parameters. Such outputs are not available from simple analytic broadband E_d or PAR light models. The availability of accurate spectral irradiances enables the use of biological models such as EcoSim [*Bissett et al*., 1999a, 1999b, 2001], which uses spectral irradiance at 5 nm resolution to model differential competition between phytoplankton functional groups according to their evolving pigment suites. Finally, inaccurate conversion of broadband irradiance to PAR for primary production calculations is obviated because both spectral and broadband quantum irradiances are a standard output of EcoLight-S, along with irradiances in energy units. This opens the door for primary production calculations to be properly done with light in quantum units.

Run time is a critical factor for large-scale ecosystem simulations. The present simulations (and those in *Mobley et al*. [2009]) indicate that the use of EcoLight-S requires no more than a few tens of percent (less than 20% in the present simulations) increase in total run time when EcoLight-S is intelligently optimized. That is to say, when EcoLight-S is called only every few hours to account for changes in the biogeochemical state of the ecosystem, when the RTE is solved only deep enough at each wavelength to account for surface boundary effects, and when the wavelength resolution is no finer than needed. This increase in run times gives increased accuracy of the light calculations, proper coupling of physics and biology, availability of ancillary optical measures of the ecosystem state, and potential improvements in ecosystem model accuracy.

Acknowledgments

The data shown in the figures are available from author C.D.M. at curtis.mobley@sequoiasci.com. Model output is in netCDF format, and includes IDL software to read those files and create the plots. The ROMS-CoSiNE-EcoLight code used in this study is available from author F.C. at fchai@maine.edu. However, the code is provided only as an example of model integration, subject to future modifications, and no support for CoSiNE or EcoLight-S will be provided. Author C.D.M. was supported in part for this work by the U.S. Office of Naval Research Ocean Optics and Biology Program, Code 322OB, under contract N00014-09-C-0044. Authors F.C. and P.X. were supported by the same program under grant N00014-08-1-0273 to F.C. We thank Steven Ackleson, Dariusz Stramski, and an anonymous reviewer for their helpful comments.

References

Bissett, W. P., M. B. Meyers, J. J. Walsh, and F. E. Mller-Karger (1994), The effects of temporal variability of mixed layer depth on primary productivity around Bermuda, *J. Geophys. Res.*, *99*(C4), 7539–7553.

Bissett, W. P., J. J. Walsh, D. A. Dieterle, and K. L. Carder (1999a), Carbon cycling in the upper waters of the Sargasso Sea: I. Numerical simulation of differential carbon and nitrogen fluxes, *Deep Sea Res., Part I*, *46*, 205–269.

Bissett, W. P., K. L. Carder, J. J. Walsh, and D. A. Dieterle (1999b), Carbon cycling in the upper waters of the Sargasso Sea: II. Numerical simulation of apparent and inherent optical properties, *Deep Sea Res., Part I*, *46*, 271–317.

Bissett, W. P., O. Schofield, S. Glenn, J. J. Cullen, W. L. Miller, A. J. Plueddemann, and C. D. Mobley (2001), Resolving the impacts and feedbacks of ocean optics on upper ocean ecology, *Oceanography*, *14*, 30–49.

Cahill, B., O. Schofield, R. Chant, J. Wilkin, E. Hunter, S. Glenn, and W. P. Bissett (2008), Dynamics of turbid buoyant plumes and the feedbacks on nearshore biogeochemistry and physics, *Geophys. Res. Lett.*, *35*, L10605, doi:10.1029/2008GL033595.

Chai, F., R. C. Dugdale, T. H. Peng, F. P. Wilkerson, and R. T. Barber (2002), One dimensional ecosystem model of the equatorial Pacific upwelling system. 1. Model development and silicon and nitrogen cycle, *Deep Sea Res., Part II*, *49*, 2713–2745, doi:10.1016/S0967-0645(02)00055-3.

Cox, C., and W. Munk (1954), Statistics of the sea surface derived from sun glitter, *J. Opt. Soc. Am.*, *44*, 838–850.

Dinniman, M. S., J. M. Klinck, and W. O. Smith Jr. (2003), Cross shelf exchange in a model of the Ross Sea circulation and biogeochemistry, *Deep Sea Res., Part II*, *50*, 3103–3120.

Evans, G. T., and J. S. Parslow (1985), A model of annual plankton cycles, *Biol. Oceanogr.*, *3*, 328–347.

Fasham, M. J. R. (1995), Variations in the seasonal cycle of biological production in subarctic oceans: A model sensitivity analysis, *Deep Sea Res., Part II*, *42*, 1111–1149.

Fasham, M. J. R., H. W. Ducklow, and S. M. McKelvie (1990), A nitrogen-based model of plankton dynamics in the oceanic mixed layer, *J. Mar. Res.*, *48*, 591–639.

Fennel, K., and J. Wilkin (2009), Quantifying biological carbon export for the northwest North Atlantic continental shelves, *Geophys. Res. Lett.*, *36*, L18605, doi:10.1029/2009GL039818.
Fennel, K., J. Wilkin, J. Levin, J. Moisan, J. O'Reilly, and D. Haidvogel (2006), Nitrogen cycling in the Middle Atlantic Bight: Results from a three-dimensional model and implications for the North Atlantic nitrogen budget, *Global Biogeochem. Cycles*, *20*, GB3007, doi:10.1029/2005GB002456.
Fennel, K., J. Wilkin, M. Previdi, and R. Najjar (2008), Denitrification effects on air-sea CO_2 flux in the coastal ocean: Simulations for the Northwest North Atlantic, *Geophys. Res. Lett.*, *35*, L24608, doi:10.1029/2008GL036147.
Fujii, M., and F. Chai (2007), Modeling carbon and silicon cycling in the equatorial Pacific, *Deep Sea Res., Part II*, *54*, 496–520.
Fujii, M., E. Boss, and F. Chai (2007), The value of adding optics to ecosystem models: A case study, *Biogeosciences*, *4*, 817–835.
Gregg, W. W., and K. L. Carder (1990), A simple spectral solar irradiance model for cloudless maritime atmospheres, *Limnol. Oceanogr.*, *35*, 1657–1675.
Hurtt, G. C., and R. A. Armstrong (1996), A pelagic ecosystem model calibrated with BATS data, *Deep Sea Res., Part II*, *43*, 653–683.
Jerlov, N. G. (1976), *Marine Optics*, Elsevier, Amsterdam.
Kyewalyanga, M., T. Platt, and S. Sathyendranath (1992), Ocean primary production calculated by spectral and broadband models, *Mar. Ecol. Prog. Ser.*, *85*, 171–185.
Lee, Z.-P., and C.-M. Hu (2006), Global distribution of Case-1 waters: An analysis from SeaWiFS measurements, *Remote Sens. Environ.*, *101*, 270–276.
Lee, Z.-P., K.-P. Du, R. Arnone, S.-C. Liew, and B. Penta (2005), Penetration of solar radiation in the upper ocean: A numerical model for oceanic and coastal waters, *J. Geophys. Res*, *110*, C09019, doi:10.1029/2004JC002780.
Lee, Z.-P., M. Jiang, C. Davis, N. Pahlevan, Y.-H. Ahn, and R. Ma (2012), Impact of multiple satellite ocean color samplings in a day on assessing phytoplankton dynamics, *Ocean Sci. J.*, *47*(3), 323–329, doi:10.1007/s12601-012-0031-5.
Lutjeharms, J. R. E., P. Penven, and C. Roy (2003), Modelling the shear edge eddies of the southern Agulhas Current, *Cont. Shelf Res.*, *23*, 1099–1115.
Marchesiello, P., J. C. McWilliams, and A. F. Shchepetkin (2003), Equilibrium structure and dynamics of the California Current System, *J. Phys. Oceanogr.*, *33*(4), 753–783.
McCreary, J. P., K. E. Kohler, R. R. Hood, S. Smith, J. Kindle, A. Fischer, and R. A. Weller (2001), Influences of diurnal and intraseasonal forcing on mixed-layer and biological variability in the central Arabian Sea, *J. Geophys. Res.*, *106*(C4), 7139–7155.
Mobley, C. D. (1994), *Light and Water: Radiative Transfer in Natural Waters*, Academic, San Diego, Calif.
Mobley, C. D. (2011a), Fast light calculations for ocean ecosystem and inverse models, *Opt. Express*, *19*(20), 18,927–18,944.
Mobley, C. D. (2011b), *EcoLight-S Users' Guide*, Sequoia Sci., Bellevue, Wash. [Available at http://www.sequoiasci.com/downloads/EcoLight-S-UsersGuide.pdf.]
Mobley, C. D., and E. Boss (2012), Improved irradiances for use in ocean heating, primary production, and photo-oxidation calculations, *Appl. Opt.*, *51*(27), 6549–6560.
Mobley, C. D., B. Gentili, H. R. Gordon, Z. Jin, G. W. Kattawar, A. Morel, P. Reinersman, K. Stamnes, and R. H. Stavn (1993), Comparison of numerical models for computing underwater light fields, *Appl. Opt.*, *32*, 7484–7504.
Mobley, C. D., L. K. Sundman, and E. Boss (2002), Phase function effects on oceanic light fields, *Appl. Opt.*, *41*(6), 1035–1050.
Mobley, C. D., L. K. Sundamn, W. P. Bissett, and B. Cahill (2009), Fast and accurate irradiance calculations for ecosystem models, *Biogeosci. Discuss.*, *5*, 10,624–10,662.
Moore, J. K., S. C. Doney, J. A. Kleypas, D. M. Glover, and I. Y. Fung (2002), An intermediate complexity marine ecosystem model for the global domain, *Deep Sea Res., Part II*, *49*, 403–462.
Morel, A. (1988), Optical modeling of the upper ocean in relation to its biogenous matter content (Case I waters), *J. Geophys. Res.*, *93*(C7), 10,749–10,768.
Morel, A., and D. Antoine (1994), Heating rate within the upper ocean in relation to its bio-optical state, *J. Phys. Oceanogr.*, *24*, 1652–1665.
Oguz, T., H. Ducklow, P. Malanotte-Rizzoli, S. Tugrul, N. P. Nezlin, and U. Unluata (1996), Simulation of annual plankton productivity cycle in the Black Sea by a one-dimensional physical-biological model, *J. Geophys. Res.*, *101*(C7), 16,585–16,599.
Ohlmann, J. C., and D. A. Siegel (2000), Ocean radiant heating. Part II: Parameterizing solar radiation transmission through the upper ocean, *J. Phys. Oceanogr.*, *30*, 1849–1865.
Oschlies, A., and V. Garçon (1998), An eddy-permitting coupled physical-biological model of the North Atlantic—Part I: Sensitivity to advection numerics and mixed layer physics, *Global Biogeochem. Cycles*, *13*(1), 135–160.
Paulson, C. A., and J. J. Simpson (1977), Irradiance measurements in the upper ocean, *J. Phys. Oceanogr.*, *7*, 952–956.
Peliz, Á., J. Dubert, D. B. Haidvogel, and B. Le Cann (2003), Generation and unstable evolution of a density-driven eastern poleward current: The Iberian Poleward Current, *J. Geophys. Res.*, *108*(C8), 3268, doi:10.1029/2002JC001443.
Shchepetkin, A., and J. C. McWilliams (1998), Quasi-monotone advection schemes based on explicit locally adaptive dissipation, *Mon. Weather Rev.*, *126*, 1541–1580.
Shchepetkin, A., and J. C. McWilliams (2003), A method for computing horizontal pressure gradient force in an oceanic model with a nonaligned vertical coordinate, *J. Geophys. Res.*, *108*(C3), 3090, doi:10.1029/2001JC001047.
Shchepetkin, A. F., and J. C. McWilliams (2005), The regional ocean modeling system (ROMS): A split-explicit, free-surface, topography-following-coordinate oceanic model, *Ocean Model.*, *9*, 347–404.
Simpson, J. J., and T. D. Dickey (1981), Alternative parameterizations of downward irradiance and their dynamical significance, *J. Phys. Oceanogr.*, *11*, 876–882.
Xiu, P., and F. Chai (2012), Spatial and temporal variability in phytoplankton carbon, chlorophyll, and nitrogen in the North Pacific, *J. Geophys. Res.*, *117*, C11023, doi:10.1029/2012JC008067.
Xiu, P., and F. Chai (2014), Connections between physical, optical and biogeochemical processes in the Pacific Ocean, *Prog. Oceanogr.*, *122*, 30–53.
Zielinski, O., A. Oschlies, and R. Reuter (1998), Comparison of underwater light field parameterizations and their effect on a 1-dimensional biogeochemical model at Station ESTOC, north of the Canary Islands, in *Proceedings Ocean Optics XIV*, pp. 1–11, P Soc. Photo-Opt. Ins., Kailua-Kona, Hawaii.